nature communications

Article

https://doi.org/10.1038/s41467-026-68771-z

Reactive oxygen species-activated bioorthogonal chemistry in living systems enabled by boronate-caged dihydrotetrazines

Received: 17 June 2025

Accepted: 16 January 2026

Published online: 10 February 2026

Check for updates

A list of authors and their affiliations appears at the end of the paper

Bioorthogonal chemistry has become a robust toolbox with growing applications in biology and medicine. To meet diverse needs in research, new types of on-demand bioorthogonal reactions capable of responding to biological triggers or exogenous stimuli are highly valuable, to achieve spatial and temporal control over reactions in living systems. Elevated levels of reactive oxygen species have been implicated in aging and multiple diseases, serving as remarkable endogenous triggers for prodrugs, probes and materials, however ROS-activated bioorthogonal ligation remains as a challenge. Here we report a reactive oxygen species activated tetrazine ligation enabled by boronate-caged dihydrotetrazines. Bioorthogonal handle tetrazines can be in situ generated from boronate-caged dihydrotetrazines upon the elevated level of hydrogen peroxide, resulting in spatiotemporal control of subsequent reactions with dienophiles. Using this strategy, a reactive oxygen species triggered construction of proteolysis targeting chimera for targeted degradation of the protein of interest bromodomain-containing protein 4 (BRD4) is successfully established by tagging boronate-caged dihydrotetrazines with a cereblon E3 ligase recruiter. Furthermore, we demonstrate a reactive oxygen species triggered tetrazine ligation enabled tumor-selective drug delivery in both living cells and mice. The present reactive oxygen species responsive delivery of cytotoxin doxorubicin via a click-to-release reaction between boronate-caged dihydrotetrazines and *trans*-cyclooctene modified doxorubicin shows excellent chemotherapeutic efficacy and safety in suppressing the growth of some tumors, superior to both direct administration of doxorubicin and reactive oxygen species sensitive prodrug of boronate-caged doxorubicin. We expect this reactive oxygen species responsive bioorthogonal reaction will offer compelling opportunities for precision therapy and provide approaches for studying pathogenesis.

e-mail: wangrui@imm.ac.cn; lpliu@imm.ac.cn

As bioorthogonal reactions have broad applications in multidisciplinary research and pharmaceutics, there is an increasing need for precise and specific control of these exogenous chemical reactions in complex living systems[1,2]. Therefore, the development of new types of on-demand bioorthogonal reactions capable of responding to stimuli holds great potential, which would enable avenues to manipulate molecules such as glycans[3], proteins[4], lipids[5], probes[6], materials[7] and prodrugs[8] in vivo, offering tools to elucidate physiological processes and providing approaches for precision therapy. Current efforts to regulate bioorthogonal reactions are mainly focused on the in situ generation of reactive reactants by means of photoclick chemistry or uncaging chemistry. For example, photoactivations of tetrazoles[9], sydnones[10], dibenzocyclopropenones[11–13], hydroxy-benzyl alcohols[14,15] with appropriate light would lead to the formation of corresponding reactive species like nitrile imines, dibenzocyclooctynes and quinone methides. Photoinduced reduction of Cu (II) to Cu (I) permits spatiotemporal control of classic click reaction between azide and alkyne[16]. On the other hand, photocatalytic oxidations of dihydrotetrazines to tetrazines have been develop, enabling precise imaging of subcellular organelles in living cells, and light-triggered hydrogel formation in living mice[17–19]. The photoclick chemistry also includes light-initiated thiol-ene[20] /alkyne[21] reactions, [3+2] cycloaddition between azides and cycloalkenes[22], as well as [4+2] cycloadditions of 9,10-phenanthrenequinones with dienophiles[23]. Meanwhile, conventional uncaging chemistry has been employed for the on-demand bioorthogonal reactions by introducing labile groups into inert precursors. However, among numerous bioorthogonal reactions, only few bioorthogonal handles have been achieved through uncaging chemistry so far. By tagging the photocaging group to triarylphosphine, light-activated Staudinger ligation has been demonstrated[24]. Tactics of photouncaging and enzymatic cleavage to generate active tetrazines or dienophiles have been demonstrated to control tetrazine ligation[4,13,25–31]. In addition to the above-mentioned uncaging chemistry by covalent labile protecting groups, noncovalent host-guest chemistry has been recently applied to regulate click reactions by encapsulating catalyst Cu (I)[32] and tetrazines[33], respectively. Despite tremendous advancements in the development of on-demand bioorthogonal chemistry, alternative benign triggers are highly favorable since many stimuli have yet to try other than light and enzymes.

Reactive oxygen species (ROS) produced by cellular oxygen metabolism play crucial roles in regulating physiological processes and maintaining homeostasis in health[34]. However, elevated levels of ROS can cause oxidative damage of biomolecules, which has been implicated in aging[35] and many diseases, such as cancer[36], inflammation[37], diabetes[38], hypertension[39] and neurodegenerative diseases[40,41]. Therefore, ROS have been used as a privileged endogenous trigger to spatiotemporally activate diagnostic or therapeutic species such as prodrugs, probes and materials at pathological sites[42,43], increasing the signal-to-noise ratio and decreasing side effects. In light of this, ROS have great promise to turn on bioorthogonal ligations, holding great potential for enhanced diagnosis and therapy. Among numerous bioorthogonal reactions, rapid tetrazine chemistry has found increasing applications in biological research, material science and medicine[44–48]. Both click[49,50] and click-to-release [51] chemistry between tetrazines and dienophiles have been widely used for the construction or activation of molecules in vivo. In this context, a ROS-triggered tetrazine ligation may offer a powerful tool for targeted interventions in oxidative stress-associated diseases.

Here, we have demonstrated a ROS-activated bioorthogonal tetrazine ligation enabled by boronate-caged dihydrotetrazines (BTz). Stable tetrazine precursors BTz have been designed and achieved by masking dihydrotetrazines with a ROS-sensitive group of aryl boronate ester via a 1,6-self-immolation linker[52,53]. Bioorthogonal handle tetrazines (Tz) can be in situ generated from boronate-caged dihydrotetrazines (BTz) upon the elevated level of hydrogen peroxide, resulting in spatiotemporal control of subsequent reactions with dienophiles. We investigate this ROS-activated bioorthogonal tetrazine chemistry in both living cells and animals. Using this strategy, a ROS-triggered in vivo construction of proteolysis targeting chimera (PROTAC) for targeted degradation of protein BRD4 is established, through a click reaction of BTz modified cereblon E3 ligase recruiter (BTz-CRBN) with trans-cyclooctene tagged JQ1 (TCO-JQ1). Furthermore, we demonstrate a ROS-on-demand tetrazine ligation enabled tumor-selective drug delivery with excellent chemotherapeutic efficacy and safety in living cells and mice. Our findings indicate that the present ROS-triggered delivery of doxorubicin via a click-to-release two-step process shows excellent chemotherapeutic efficacy and safety for some tumors, superior to both the direct administration of doxorubicin and ROS-sensitive boronate-caged doxorubicin.

Results and discussion

Synthesis of ROS-responsive tetrazine precursors

Hydrogen peroxide (H_2O_2) is one of the most abundant reactive oxygen species (ROS) in humans and it has been reported that the amount of H_2O_2 in some tumor environments could reach over 100 times higher compared to normal tissues[54]. Given this, we envisioned that the elevated level of H_2O_2 could serve as a benign endogenous trigger to regulate the tetrazine ligation in vivo. On the basis of our previous experience with photouncaging tetrazine chemistry[25,55], ROS-sensitive precursor **1** of 6-methyl-3-phenyl-1,2,4,5-tetrazine **1a** has been designed and achieved by masking the corresponding dihydrotetrazine with a highly H_2O_2-selective phenyl pinacol boronate[52,53] (see Supplementary synthetic method). Upon reaction with elevated H_2O_2, we expected that phenyl pinacol boronate-caged 6-methyl-3-phenyl-1,4-dihydro-1,2,4,5-tetrazine **1** would be oxidized to form the intermediate phenol, subsequently releasing the desired tetrazine (Tz) **1a** via a 1,6-elimination along with side products of carbon dioxide (CO_2) and quinone methide (Fig. 1a). To reach this goal, we first evaluated the biocompatibility of boronate-caged dihydrotetrazine (BTz) **1** in vitro, and treated compound **1** with a common cell culture DMEM complete media at 37 °C. HPLC revealed that trace amount of tetrazine **1a** was observed in 4 h and less than 10% of **1a** was detected after 12 h (Fig. S1), which suggested that BTz **1** was compatible with the biologically relevant aqueous solution. As we initially anticipated that only the elevated level of H_2O_2 would trigger the oxidative formation of tetrazines from boronate-caged dihydrotetrazines. To test this hypothesis, we next explored the reactivity of BTz **1** with different concentrations of H_2O_2 in PBS solution and samples were taken from the reaction mixture after 4 h and examined by HPLC (Fig. 1b). Without H_2O_2, negligible amount of tetrazine **1a** was observed and very little of tetrazine **1a** (20% yield, 4 h) was formed with a normal physiological concentration of H_2O_2 (10 μM). However, 59% yield of tetrazine **1a** was generated from its precursor of BTz **1** after 4 h when using 100 μM of H_2O_2, and an improved yield of 75% was obtained by extending the reaction duration for 12 h (red, Fig. 1c). In contrast, only 4% of **1a** was observed without H_2O_2 (blue, Fig. 1c). These findings indicated that the present ROS-responsive boronate-caged dihydrotetrazine was highly dose-dependent, therefore larger amounts of tetrazine **1a** were obtained from BTz **1** when we increased the concentrations of H_2O_2 to 200 μM (72% yield, 4 h) and 500 μM (94% yield, 4 h). Hence, we anticipated that the endogenous high level of H_2O_2 at some pathological sites would be able to spatiotemporally trigger the oxidative formation of tetrazines from BTz in vivo. HPLC analysis in Fig. 1d revealed that boronate ester group within BTz **1** were fully hydrolyzed to boronic acid (see Supplementary high-resolution mass spectrometry) in PBS solution, which has been reported capable of responding to H_2O_2[52]. Once BTz **1** was treated with 100 μM of H_2O_2, a peak of dihydrotetrazine **1b** was observed by HPLC (Fig. 1d), suggesting the ROS-

activated formation of tetrazine **1a** from BTz **1** may proceed through the intermediate of dihydrotetrazine **1b**.

Although phenyl pinacol boronates are widely used in chemical biology[52,53], purification of such compounds by silica gel column chromatography without distinct loss of yields is a known challenge. A recent report reveals that aryl boronic acid 1,1,2,2-tetraethylethylene glycol esters can be obtained in high yields after purification by column chromatography on silica gel[56]. We wondered whether phenyl boronic acid 1,1,2,2-tetraethylethylene glycol ester-caged dihydrotetrazine could be a suitable substrate for the anticipated H_2O_2-triggered tetrazine ligation. Given this, we have synthesized the phenyl boronic acid 1,1,2,2-tetraethylethylene glycol ester-caged 6-methyl-3-phenyl-1,4-dihydro-1,2,4,5-tetrazine **2** (see Supplementary synthetic method). However, BTz **2** showed sluggish reactivity towards 100 μM of H_2O_2 in PBS solution at 37 °C and 33% yield of tetrazine **1a** was detected after 12 h (Fig. S2). Therefore, we chose the H_2O_2-sensitive phenyl pinacol boronate to further extend the scope of BTz (Fig. 1e). Since tetrazine ligations between tetrazines and dienophiles undergo inverse electron demand Diels–Alder reactions, to enhance the reactivity of cycloadditions, more electron-deficient substituents on boronate-caged dihydrotetrazines **3** and **4** have been examined. To our delight, both 3,6-diphenyl-1,2,4,5-tetrazine **3a** (66% yield, 8 h) and 6-methyl-3-(pyridin-2-yl)−1,2,4,5-tetrazine **4a** (91% yield, 4 h) could be oxidative generated from corresponding BTz **3** and BTz **4** in good yields (Figs. S3 and S4). Considering the introduction of functional groups on aryl boronate-caged dihydrotetrazines may facilitate their applications, we chose BTz **1** as a standard substrate for the subsequent explorations.

H_2O_2-dependent targeted protein degradation

As tetrazine precursors of phenyl pinacol boronate-caged dihydrotetrazines (BTz) can be activated by high level of H_2O_2 in biorelevant aqueous PBS solution, we next aimed at H_2O_2-dependent tetrazine ligations and explored their applications. Proteolysis targeting chimera (PROTAC) has been extensively exploited in drug discovery, which can degrade specific proteins of interest in a catalytic manner. Tetrazine ligations have been previously implemented to synthesize or activate PROTAC[57,58], Thus we hypothesized that the newly developed boronate-caged dihydrotetrazines could enable a H_2O_2-dependent PROTAC, which holds great potential for precision cancer therapy. For this reason, we decided to explore a H_2O_2-dependent construction of

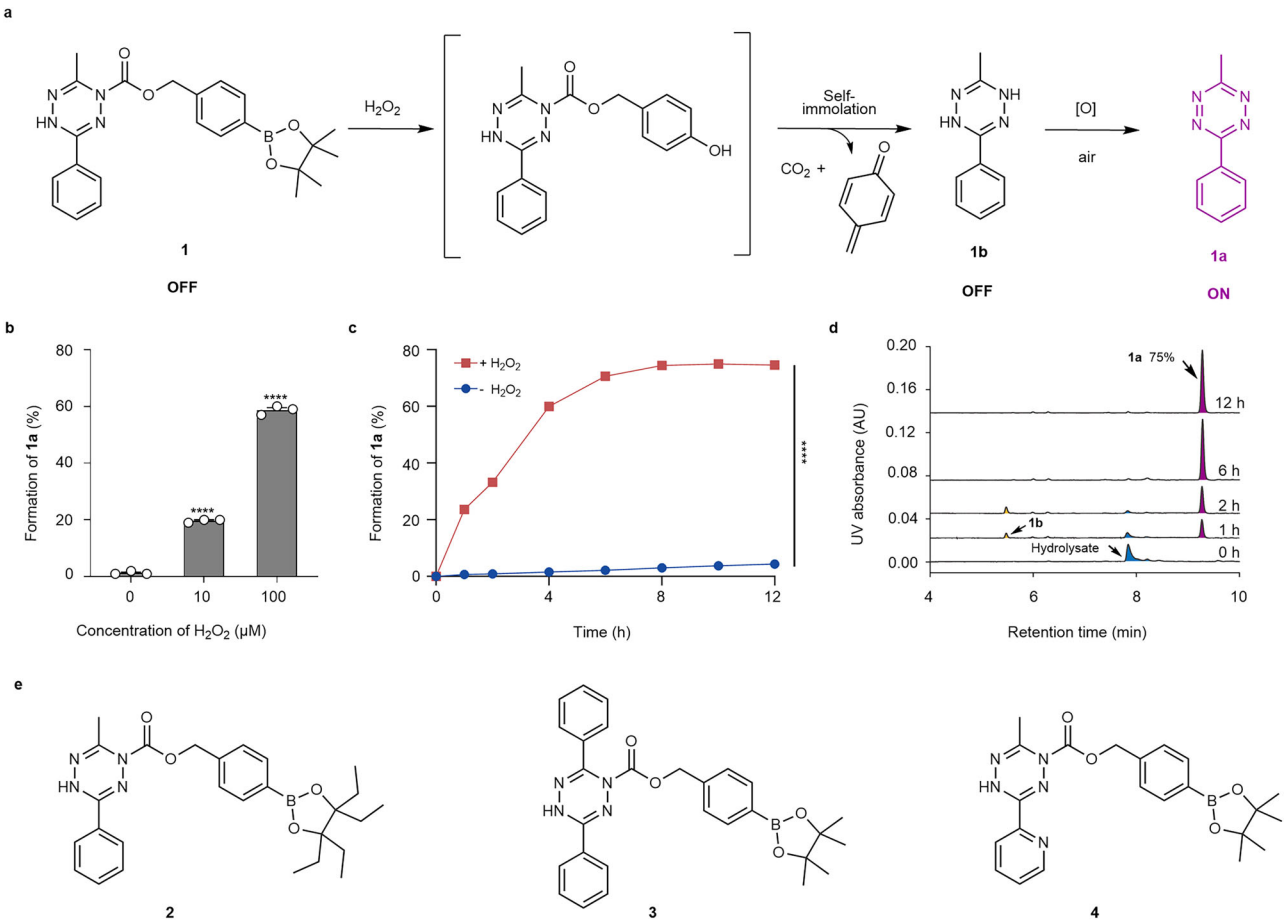

Fig. 1 | ROS-activated formation of tetrazines from boronate-caged dihydrotetrazines. a H_2O_2-activated formation of tetrazine **1a** from BTz **1**. **b** The reaction was carried out by incubating **1** (5 μM) without or with H_2O_2 (10 μM, 100 μM) in PBS solution (containing 1% DMSO) at 37 °C for 4 h. Samples were taken from the reaction mixtures at 4 h and examined by high performance liquid chromatography (HPLC) (absorbance monitored at 254 nm). Data were presented as mean ± standard error of the mean (SEM), open circles indicate independent experiments ($n = 3$). Statistically significant differences between no H_2O_2 treatment and other treatments were indicated using an independent *t*-test (two-tailed): $^{****}P < 0.0001$. **c** The reaction was carried out by incubating **1** (5 μM) without or with H_2O_2 (100 μM) in PBS solution (containing 1% DMSO) at 37 °C for 12 h. Samples were taken from the reaction mixtures at different time points and examined by HPLC. Spectra with and without H_2O_2 for 12 h (absorbance monitored at 254 nm). Data were presented as mean ± standard error of the mean (SEM) ($n = 3$ independent experiments). Statistically significant differences between no H_2O_2 treatment and 100 μM H_2O_2 treatment were indicated using a two-way analysis of variance (ANOVA) with a Tukey post-hoc test ($n = 3$). $^{****}P < 0.0001$. **d** Incubating **1** (5 μM) with 100 μM of H_2O_2 in PBS solution (containing 1% DMSO) at 37 °C. Samples were taken at 0 h, 1 h, 2 h, 6 h and 12 h, then examined by HPLC (absorbance monitored at 254 nm). AU, absorbance unit. **e** Boronate-caged dihydrotetrazines. Source data are provided as a Source Data file.

https://doi.org/10.1038/s41467-026-68771-z

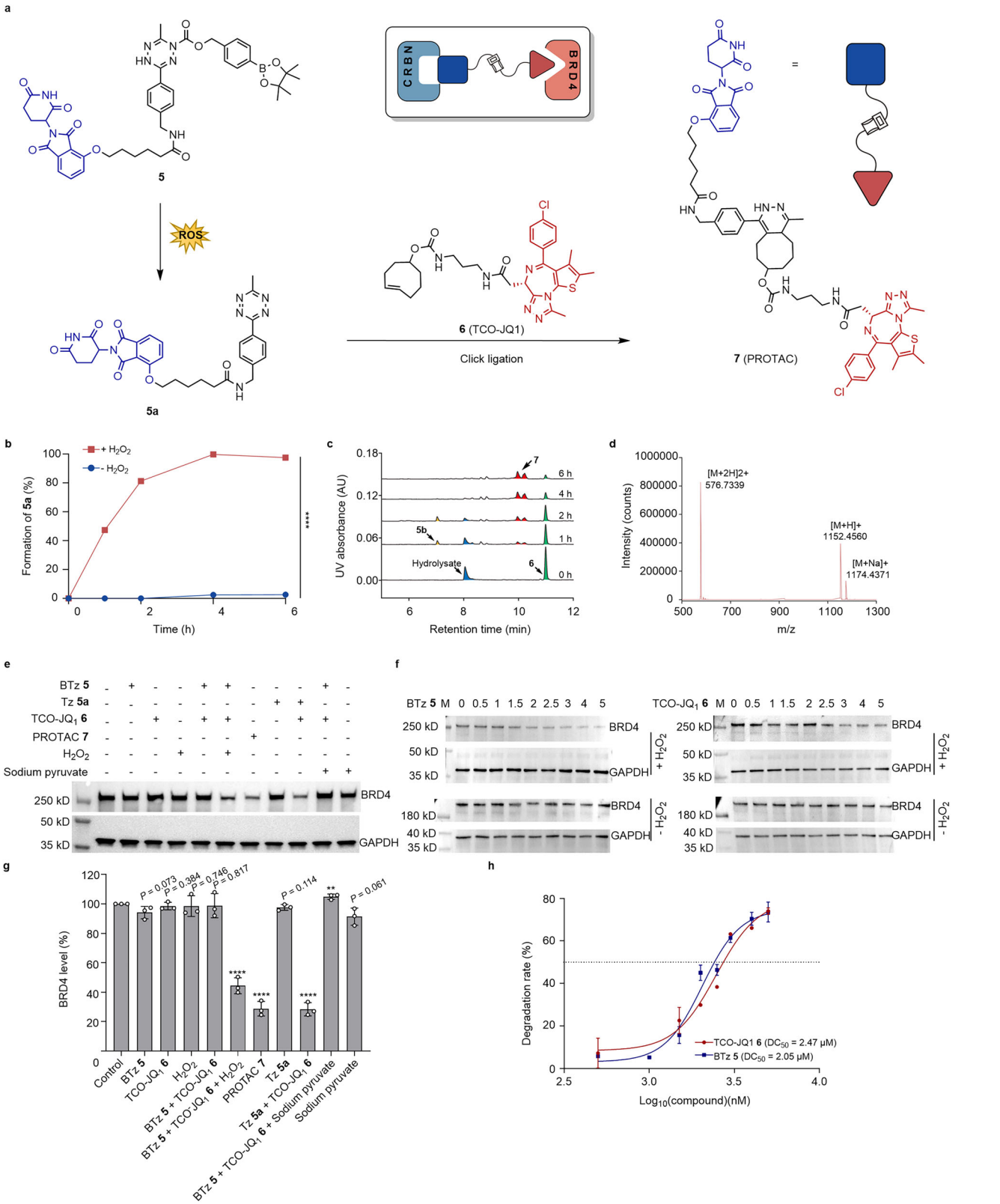

PROTAC in cancer cells. Therefore, boronate-caged dihydrotetrazine-tagged E3 ligase recruiting ligand thalidomide **5** was synthesized, which would recruit E3 ubiquitin ligase cereblon (CRBN). We anticipated that BTz **5** would be oxidized to tetrazine **5a** in the presence of the elevated level of H_2O_2, then underwent a click ligation reaction with TCO-JQ1 **6** to generate the PROTAC **7**, resulting in the recruitment of CRBN to degrade the targeted BRD4 protein (Fig. 2a).

For this purpose, we first investigated the oxidative formation of tetrazine **5a** from BTz **5** (5 μM) in PBS solution. Samples were taken from the reaction mixture at different time points and examined by HPLC. As expected, the oxidative yields of tetrazine **5a** from its precursor BTz **5** exhibited a strong dose-dependent relationship with the concentration of H_2O_2, and only trace amount of **1a** (3%, 6 h) was observed without H_2O_2 (blue, Fig. 2b). However, compared to BTz **1**, a

Fig. 2 | H_2O_2-dependent construction of PROTAC to degrade BRD4 protein in A549 cancer cell. a Upon exposure to high concentrations of H_2O_2, BTz-tagged E3 ligase recruiting ligand thalidomide **5** will be oxidized to Tz-thalidomide **5a**, which can react with TCO-JQ1 **6** to form PROTAC **7** for the targeted degradation of protein BRD4 (Created in BioRender. lab, L. (2026) https://BioRender.com/bm3fqz5). **b** The reaction was carried out by incubating **5** (5 μM) without or with H_2O_2 (100 μM) in PBS solution (containing 1% DMSO) at 37 °C for 6 h. Samples were taken from the reaction mixtures at different time points and examined by HPLC. Spectra with and without H_2O_2 for 6 h (absorbance monitored at 254 nm). Data were presented as mean ± standard error of the mean (SEM) ($n = 3$). Statistically significant differences between no H_2O_2 treatment and 100 μM H_2O_2 treatment were indicated using a two-way analysis of variance (ANOVA) with a Tukey post-hoc test ($n = 3$). $^{****}P < 0.0001$. **c** The reaction was carried out by incubating **5** (5 μM) and TCO-JQ1 **6** (5 μM) with 100 μM of H_2O_2 in PBS solution (containing 1% DMSO) at 37 °C. Samples were taken from the reaction mixtures at different time points and examined by HPLC. (absorbance monitored at 254 nm). **d** High resolution mass spectrometry (HRMS) of PROTAC **7**. **e** Western blot assay of PROTAC-mediated BRD4 degradation in A549 cells. Cells were treated with TCO-JQ1 **6** (5 μM) for 6 h, followed by incubation with **5** (5 μM) or **5a** (5 μM) in the presence or absence of 10 mM sodium pyruvate or 100 μM of H_2O_2 at 37 °C for 18 h. **f** Dose-dependent degradation of BRD4. **g** Effect of different compound on BRD4 degradation in A549 cells. Data were presented as mean ± standard error of the mean (SEM), open circles indicate independent experiments ($n = 3$ biologically independent samples). Statistically significant differences between control and other treatments were indicated using an independent *t*-test (two-tailed): $^{****}P < 0.0001$, $^{**}P < 0.01$. **h** Degradation rate of BRD4 in A549 cell line. Data were presented as mean ± standard error of the mean (SEM) ($n = 3$ biologically independent samples). Source data are provided as a Source Data file.

higher yield of 98% was obtained from BTz **5** under the same reaction conditions (red, Figs. 2b and S5), which shown that substitutions on the phenyl ring of dihydrotetrazines could influence the tetrazine formation kinetics. Encouraged by this result, we next investigated the H_2O_2-driven click reaction between BTz **5** and TCO-JQ1 **6** in PBS solution. Upon 100 μM of H_2O_2, isomers of PROTAC **7** were rapidly detected by HPLC (Fig. 2c) and confirmed by high-resolution mass spectrometry (Fig. 2d). For comparison, no PROTAC **7** was formed in the absence of H_2O_2 (Fig. S6). Therefore, we anticipated that the endogenous high level of H_2O_2 at some pathological sites would be able to spatiotemporally trigger the oxidative formation of PROTAC **7** in vivo.

Encouraged by the in vitro results, we next investigated the intracellular formation of active PROTAC **7** in A549 cells. As shown in Fig. S7, we analyzed the amount of PROTAC **7** in cell lysates after co-treatment with BTz **5**, TCO-JQ1 **6**, and H_2O_2 (100 μM) for 5 h, and 91% yield of **7** was observed, which is compared to the positive control group treated with tetrazine **5a** and TCO-JQ1 **6**. In contrast, almost no PROTAC **7** formation was detected in the presence of the ROS scavenger sodium pyruvate[59], indicating that the reaction is H_2O_2-dependent. On this basis, we next evaluated the H_2O_2-activated tetrazine ligations between BTz **5** and TCO-JQ1 **6** in living cells to degrade BRD4 protein. We selected two distinct cell lines that overexpressed BRD4 protein including A549 and HeLa. Cells were treated with TCO-JQ1 **6** (5 μM) for 6 h followed by adding tetrazine **5a** (5 μM) or BTz **5** (5 μM) along with or without 10 mM sodium pyruvate or 100 μM of H_2O_2 for 18 h. As shown in Fig. 2e, f, western blot analysis demonstrated that no obvious degradation of BRD4 was observed when cells were treated with a mixture of BTz **5** (5 μM) and TCO-JQ1 **6** (5 μM). However, by co-treatment with 100 μM of H_2O_2, notable 60% of BRD4 was degraded, which was comparable to the result (71% of BRD4 degradation) of positive controls treated with either PROTAC **7** or the combination of tetrazine **5a** (5 μM) and TCO-JQ1 **6** (5 μM). As sodium pyruvate is known to scavenge the ROS within living cells[59], BRD4 proteins were not obviously degraded when we treated cells with sodium pyruvate (10 mM), BTz **5** (5 μM) and TCO-JQ1 **6** (5 μM). Additionally, we have shown that BTz **5** (5 μM), TCO-JQ1 **6** (5 μM) or tetrazine **5a** (5 μM) alone was not able to alter the level of BRD4 proteins in cells (Figs. 2e, g and S8). Furthermore, we established a series of concentration gradients to explore the BRD4 protein degradation process in detail, and experiments were conducted using various concentrations of BTz **5** or TCO-JQ1 **6**. In a similar manner, cells were treated with TCO-JQ1 **6** for 6 h, followed by the addition of BTz **5** (5 μM) without or with100 μM of H_2O_2 for 18 h. As shown in Fig. 2f, h, the degradation of BRD4 turned out to be dose-dependent of BTz **5** and TCO-JQ1 **6** in A549 cell line with DC_{50} values of 2.05 μM and 2.47 μM, respectively. These results suggested that the boronate-caged dihydrotetrazine could enable a H_2O_2-dependent PROTAC to degrade BRD4 protein in different cancer cell lines and we expected such a strategy can be further utilized to degrade other proteins of interest.

ROS-responsive delivery of doxorubicin in cancer cells

Having successfully achieved a H_2O_2-dependent PROTAC in living cells via a tetrazine click reaction, we further incorporated boronate-caged dihydrotetrazines with click-to-release chemistry. This approach would allow the targeted liberation of drugs at pathological sites with high levels of H_2O_2. Thus, we synthesized a prodrug trans-cyclooctene modified doxorubicin (TCO-Dox) **8** and hypothesized that cytotoxin doxorubicin (Dox) would be released via a H_2O_2-triggered click-to-release reaction between BTz **1** and TCO-Dox **8** (Fig. 3a, left)[51]. For comparison, a H_2O_2-sensitivity prodrug boronate-caged doxorubicin (B-Dox) **9** has been evaluated as well (Fig. 3a, right). We first investigated the H_2O_2-triggered release of Dox in PBS solution, which was carried out by incubating BTz **1** (5 μM) and TCO-Dox **8** (1.5 μM) with 100 μM of H_2O_2 in PBS solution (containing 1% DMSO) at 37 °C. As shown in Fig. 3b, HPLC analysis revealed that BTz **1** exhibited rapid reaction kinetics with TCO-Dox **8** in the presence of H_2O_2 (100 μM), showing an efficient liberation of Dox. Encouraged by these results, we next investigated the anticipated H_2O_2-responsive release of Dox in MC38 colon cancer cells. Comprehensive cytotoxicity assessments across a range of concentrations of various treatments have been performed (Figs. 3c and S10). As shown in Fig. 3c, treatment of MC38 cells with Dox resulted in cytotoxic effects with an IC_{50} of 2.13 μM and treatment with the combination of BTz **1** and TCO-Dox **8** in the presence of 100 μM H_2O_2 showed a comparable IC_{50} of 3.09 μM. However, treatments with either the combination of BTz **1** + TCO-Dox **8**, BTz **1** + H_2O_2 (100 μM) or TCO-Dox **8** + H_2O_2 (100 μM) exhibited minimal cytotoxic effect. As shown in Fig. 3d, when MC38 colon cancer cells were treated with either BTz **1** (13.2 μM) or TCO-Dox **8** (4 μM) alone, or their combination, did not affect cell viability after 18 h of incubation. However, treatment with a mixture of BTz **1** (13.2 μM), TCO-Dox **8** (4 μM) and 100 μM of H_2O_2, cell viability was dramatically decreased to 49%, which was almost identical to the direct administration of cytotoxin Dox (4 μM) under the same conditions. In the presence of H_2O_2 (100 μM), no significant loss of cell viability was observed with either TCO-Dox **8** (4 μM), BTz **1** (13.2 μM) or a routine H_2O_2-sensitivity prodrug B-Dox **9** (4 μM) alone. These results indicate that boronate-caged dihydrotetrazines can be used for the ROS-responsive drug delivery in living cancer cells to kill some tumors.

Tumor-selective drug delivery in mice model

Encouraged by the excellent therapeutic efficiency of H_2O_2-activated drug delivery in cancer cells, we next investigated the therapeutic potential of BTz in a murine model (Fig. 4). First of all, we quantified the H_2O_2 levels in tumor and surrounding muscles harvested from MC38 tumor-bearing male C57BL/6 mice ($n = 3$ biologically independent samples) upon reaching a tumor volume of 200 mm^3. As shown in Fig. S11a, the H_2O_2 concentration in tumors reached ~1.9 μmol/g, which is about 8.7-fold higher than that of surrounding normal muscle tissues. The elevated level of H_2O_2 at the tumor site should be sufficient

https://doi.org/10.1038/s41467-026-68771-z

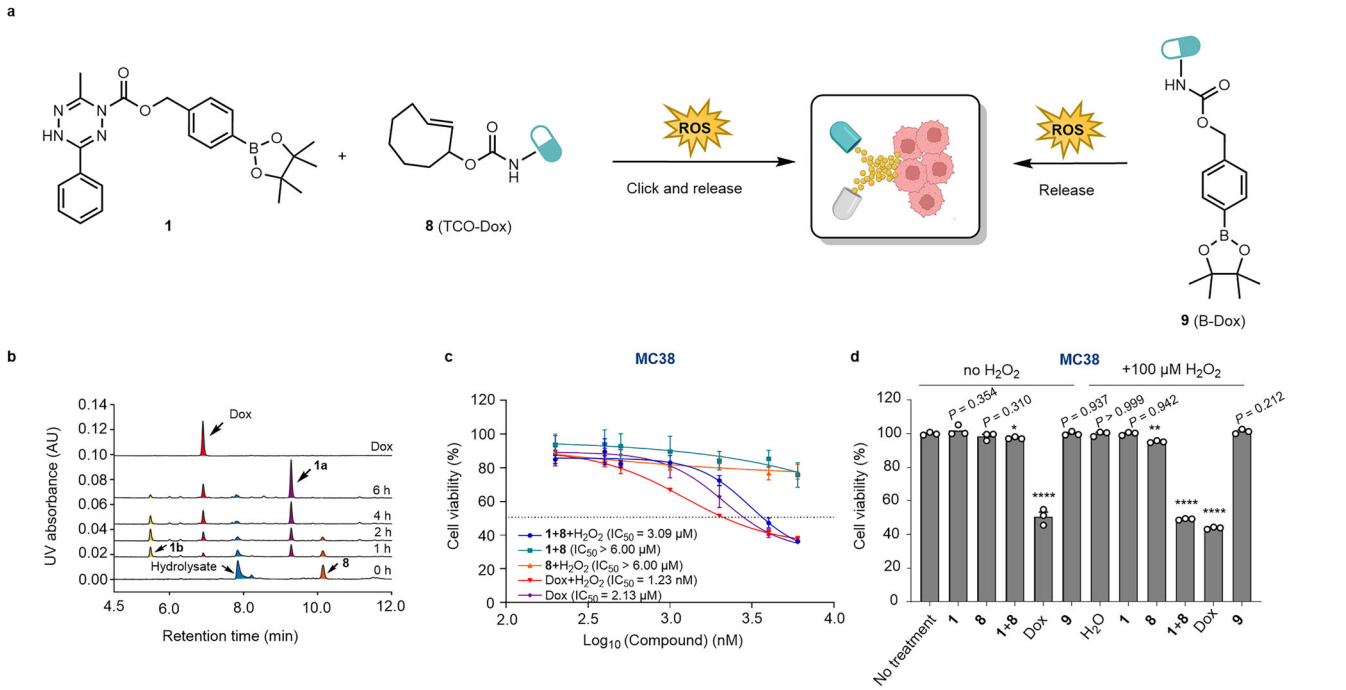

Fig. 3 | ROS-responsive delivery of doxorubicin in cancer cells. a ROS-activated tetrazine ligation enabled delivery of Dox from TCO-Dox **8** via a click-to-release two-step process is shown on the left, and direct activation of ROS-sensitive B-Dox is shown on the right. Dox, doxorubicin; TCO-Dox, *trans*-cyclooctene modified doxorubicin; B-Dox, boronate-caged doxorubicin (Created in BioRender. lab, L. (2026) https://BioRender.com/bm3fqz5). **b** The reaction was carried out by incubating **1** (5 μM) and TCO-Dox **8** (1.5 μM) with 100 μM of H_2O_2 in PBS solution (containing 1% DMSO) at 37 °C. Samples were taken from the reaction mixtures at different time points and examined by HPLC. (absorbance monitored at 254 nm). **c** IC_{50} curves of MC38 cells treated with BTz **1** (3.3 eq) + TCO-Dox **8** (1 eq) + H_2O_2 (100 μM), BTz **1** (3.3 eq) + TCO-Dox **8** (1 eq), TCO-Dox **8** + H_2O_2 (100 μM), Dox + H_2O_2 (100 μM) or Dox at 37 °C for 18 h. Data were presented as mean ± SEM ($n = 3$ biologically independent samples). **d** Cell viability of MC38 cells after treatments with BTz **1** (13.2 μM), TCO-Dox **8** (4 μM), Dox (4 μM), or B-Dox **9** (4 μM) with or without H_2O_2 (100 μM), followed by incubation at 37 °C for 18 h. Data were presented as mean ± standard error of the mean (SEM), open circles indicate independent experiments ($n = 3$ biologically independent samples). Statistically significant differences in cell viability between no treatment and other treatments were indicated using an independent *t*-test (two-tailed): $^{****}P < 0.0001$, $^{**}P < 0.01$, $^{*}P < 0.05$. Source data are provided as a Source Data file.

to trigger the conversion of BTz **1** to tetrazine **1a** according to the above in vitro experiments, allowing the subsequent reaction with TCO-Dox to release the cytotoxin doxorubicin.

To test this hypothesis, we conducted a comprehensive biodistribution study in MC38 tumor-bearing mice treated with TCO-Dox **8**, free Dox, the combination of BTz **1** + TCO-Dox **8**, or the combination of BTz **1** + TCO-Dox **8** + intratumoral catalase. When the tumor volume reached ~200 mm^3, the mice were randomly divided into four experimental groups ($n = 3$ per group). Group **8** received an intraperitoneal (i.p.) injection of 28.7 μmol·kg^{-1} TCO-Dox **8** and a subcutaneous (s.c.) injection of solvent control. Group Dox received an i.p. injection of 8.6 μmol·kg^{-1} Dox and a s.c. injection of the solvent control. Group **1**+**8** received an i.p. injection of 28.7 μmol·kg^{-1} TCO-Dox **8**, followed by a s.c. injection of 115.2 μmol·kg^{-1} BTz **1** near the tumor site after a 20-min interval. Group **1**+**8**+catalase received the same dosing regimen as Group **1**+**8**, but with an intratumoral (i.t.) injection of catalase (0.3 μg) administered immediately prior to BTz **1** injection. To sustain a reproduced H_2O_2 concentration in tumor, a second i.t. injection of catalase (0.3 μg) was given at 12 h post initial treatment. All mice were euthanized after 24 h treatment and major tissues (heart, liver, kidneys, and tumor) were then collected for LC-MS/MS analysis (Fig. 4b, c). In Group **8**, TCO-Dox has been mainly observed in tumor and liver tissues while not detectable in the heart and kidneys, which is consistent with typical pharmacokinetics involving hepatic processing and passive accumulation in tumors (Fig. 4b). In stark contrast, Group **1**+**8** showed nearly undetectable levels of both BTz **1** and TCO-Dox **8** in all tissues. This near-complete clearance is consistent with the efficient consumption of TCO-Dox **8** via the bioorthogonal click-to-release reaction, rather than solely natural clearance processes. For comparison, the TCO-Dox biodistribution in the group of **1**+**8**+catalase, where intratumoral H_2O_2 was dramatically decreased (Fig. S11a), displayed a similar pattern to those of **8** alone, indicating that the biorthogonal click-to-release reaction was impeded by the reduced amount of H_2O_2. Correspondingly, Dox release profiles revealed the critical role of H_2O_2 in tumors (Fig. 4c). The group of TCO-Dox **8** alone yielded negligible Dox systemically, while a direct administration of free Dox has been mainly observed in liver, heart and kidneys. Notably, the combination group of **1**+**8** exhibited markedly enhanced tumor-selective delivery of cytotoxin doxorubicin compared to the combination of **1**+**8**+catalase, further validating the H_2O_2-activated click-to-release for drug delivery at tumor site. Overall, a tumor-selective drug delivery in mice model has been established and we envisioned this ROS-responsive click-to-release reaction between BTz and TCO-caged cytotoxins hold great potentials for precision cancer therapeutic.

We next evaluated the in vivo therapeutic efficacy of BTz **1** plus TCO-Dox **8** combination compared with that of free Dox and negative control groups in a MC38 tumor-bearing male C57BL/6 mouse model. When the tumor volume reached 50–100 mm^3, MC38 tumor-bearing mice were randomly divided into seven groups ($n = 5$/group). The treatment group (G5) received an intraperitoneal injection (i.p.) of 28.7 μmol·kg^{-1} TCO-Dox **8**, subsequently, after a 20-min interval, a subcutaneous injection (s.c.) of 115.2 μmol·kg^{-1} BTz **1** was given near the tumor site. For comparative analysis, the remaining 6 groups were treated as follows. The interval between the two injections was maintained at 20 min (Fig. 4a). To rule out the potential influence of the solvent and the procedure of subcutaneous injection near the tumor

https://doi.org/10.1038/s41467-026-68771-z

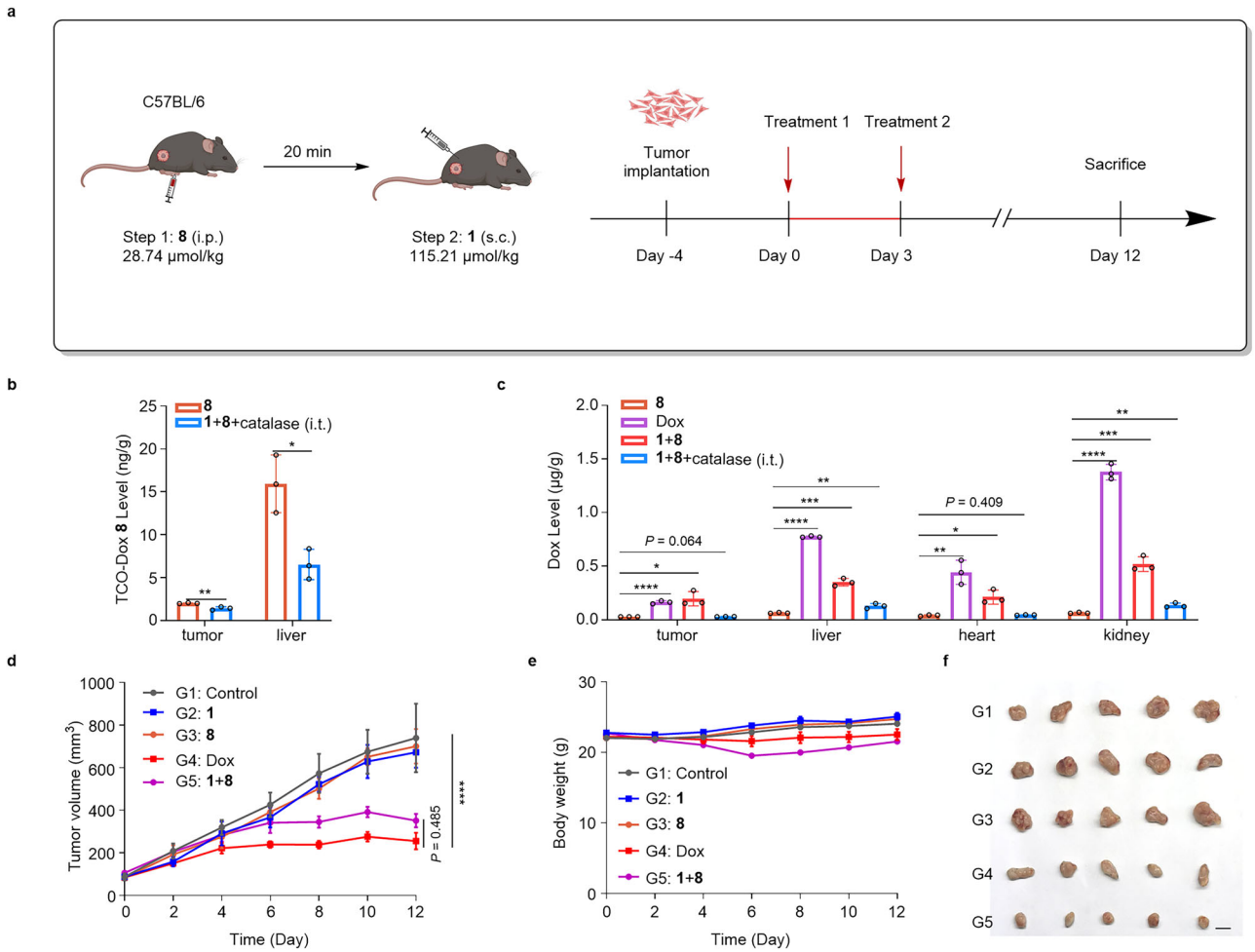

Fig. 4 | Therapeutic efficacy of prodrug activation in MC38 subcutaneous tumor model. a Flowchart showing the course of treatment. The mice received two treatment courses on day 0 and 3. Tumor volume and body weight were measured every 2 d (Created in BioRender. lab, L. (2025) https://BioRender.com/bm3fqz5). **b** LC-MS/MS analysis of biodistribution of TCO-Dox **8** in different tissues of mice treated with either **8** alone or **1** + **8**+catalase after 24 h. Data were presented as mean ± standard error of the mean (SEM), open circles indicate independent experiments ($n = 3$ biologically independent samples). Statistically significant differences analysis was indicated using an independent t-test (two-tailed): $^{**}P < 0.01$, $^{*}P < 0.05$. **c** LC-MS/MS analysis of biodistribution of Dox in different tissues of mice treated with either TCO-Dox **8**, Dox, **1** + **8**, or **1** + **8**+catalase after 24 h. Data were presented as mean ± standard error of the mean (SEM), open circles indicate independent experiments ($n = 3$ biologically independent samples). Statistically significant differences analysis were indicated using an independent t-test (two-tailed): $^{****}P < 0.0001$, $^{***}P < 0.001$, $^{**}P < 0.01$, $^{*}P < 0.05$. **d** Curve of the tumor volume change within 12 d ($n = 5$ biologically independent samples). Tumor volume was calculated as $V = 0.5 \times (\text{major axis}) \times (\text{minor axis})^2$. Statistically significant differences are determined by two-way analysis of variance (ANOVA) with a Tukey post-hoc test. $^{****}P < 0.0001$. **e** Curve of the body weight change within 12 d ($n = 5$ biologically independent samples). **f** Photographs of tumor samples dissected after treatment for 12 d. Scale bar: 10 mm. All data were presented as mean ± standard error of the mean (SEM). Source data are provided as a Source Data file.

site, appropriate solvents were administered to these control groups: G1 received solvent (i.p.) + solvent (s.c.), G2 received solvent (i.p.) + 115.2 μmol·kg^{-1} **1** (s.c.), G3 received 28.7 μmol·kg^{-1} **8** (i.p.) + solvent (s.c.), G4 received 8.6 μmol·kg^{-1} Dox (i.p.) + solvent (s.c.), G6 received 28.7 μmol·kg^{-1} Dox (i.p.) + solvent (s.c.), and G7 received 8.6 μmol·kg^{-1} **8** (i.p.) + 115.2 μmol·kg^{-1} **1** (s.c.). The mice was received two treatment courses on day 0 and 3.

Tumor volume and body weight were measured every 2 d. After 2 treatment courses, mice in G2 and G3 groups treated with BTz **1** or TCO-Dox **8** alone exhibited a rapid tumor growth rate comparable to that of the untreated G1 group. Notably, the body weight of these mice remained stable without significant changes, indicating that both BTz **1** and TCO-Dox **8** demonstrate high biocompatibility in C57BL/6 mice. For the positive control G4 group, mice treated directly with Dox (8.6 μmol·kg^{-1}) exhibited significant inhibition of tumor growth. However, a notable decrease in body weight was observed compared to other groups. Notably, mice in the G5 group, which received a combination treatment (28.7 μmol·kg^{-1} **8** + 115.2 μmol·kg^{-1} **1**) showed superior tumor suppression, achieving a tumor growth inhibition (TGI) value as high as 66%. This is comparable to the results observed in the positive control G4 group, underscoring the efficacy of tumor-selective drug delivery in vivo. In addition, mice in the G5 group exhibited stable body weight, further indicating the excellent biocompatibility and safety profile of our prodrug approach. This promising strategy exhibits significant potential to alleviate the adverse effects associated with chemotherapy. Consequently, we have adopted a tumor-selective drug delivery strategy to minimize the side effects of Dox (Fig. 4d, e).

To further substantiate the safety and efficacy of our proposed scheme, G6 and G7 groups play a crucial role. Mice in the G6 group received a high dosage of Dox (28.7 μmol·kg^{-1}), exhibited significant weight loss and all succumbed by day 6, indicating that TCO-Dox **8** has lower toxicity than Dox at the same dosage. Mice in the G7 group, administered a low dose of TCO-Dox **8** equivalent to that of the G4

group (8.6 μmol·kg^{-1}), showed only modest inhibition of tumor growth, with the effect being less pronounced (Fig. S12). Ultimately, these mice were sacrificed on day 12, and their tumors were excised and photographed. The results were consistent with the tumor volume analysis (Fig. 4f).

In summary, we have developed an on-demand bioorthogonal tetrazine ligation in response to the endogenous elevated level of hydrogen peroxide. Masking dihydrotetrazines with a H_2O_2-sensitive group aryl boronate ester through a self-immolation linker leads to stable tetrazine precursors BTz, which undergo controllable tetrazine ligations with dienophiles under oxidative stress. This ROS-activated bioorthogonal chemistry has been implemented to spatiotemporally manipulate molecules of interest both in vitro and in vivo. Using this strategy, we have demonstrated a ROS-triggered construction of PROTAC in living cells through a click reaction between BTz-tagged thalidomide and TCO-modified ligand JQ1. We anticipate this on-demand degradation of targeted proteins would find promising applications in the study and treatment of cancers and other diseases. By involving BTz with the click to release strategy in tetrazine chemistry, tumor-selective delivery of chemotherapeutic doxorubicin has been established and this approach exhibits superior chemotherapeutic efficacy and safety in inhibiting the growth of tumors, outperforming both direct drug administration of doxorubicin and ROS-responsive prodrug boronate-caged doxorubicin. We envision ROS-triggered bioorthogonal reactions between tetrazines and dienophiles can be used for the construction or activation of other molecules of interest, such as probes, proteins and drugs. We believe that the ROS-activated tetrazine chemistry will find wide applications in biological research, medicine and material science in the future, as oxidative stress is closely associated with aging and many other diseases, like inflammation, diabetes and cardiovascular or neurological diseases. Efforts to develop on-demand bioorthogonal chemistry are currently ongoing in our laboratory.

Methods

H_2O_2-activated tetrazines formation from boronate-caged dihydrotetrazines

A solution of the respective boronate-caged dihydrotetrazine (BTz 2-5, 5 μM) in PBS (containing 1% DMSO) was treated with H_2O_2 (100 μM) and incubated at 37 °C. Samples were withdrawn from the reaction mixture at designated time points and analyzed by HPLC. HPLC analysis was performed on an Xbridge C18 column (4.6 × 150 mm, 5 μm) using a gradient of water (0.1% TFA) and acetonitrile at a flow rate of 1 mL/min (column temperature: 40 °C), with detection at 254 nm.

Cell culture

A549 (1101HUM-PUMC000002) human lung cancer cell line and MC38 (1101MOU-PUMC000523) mouse colon carcinoma cell line was from Cell Resource Center, Institute of Basic Medical Sciences, Chinese Academy of Medical Sciences (NICR). HeLa (CRM-CCL-2) human cervical cancer cell line was from American Type Culture Collection. Cells were cultured at 37 °C in a humidified atmosphere containing 5% CO_2 in DMEM with high glucose (PM150210, Pricella), 10% FBS (10099-141C, gibco), 1% Penicillin and Streptomycin (15140-122, gibco) were added additionally.

Cell viability assay

MC38 cells were seeded in 96-well plates at 8×10^3 cells per well in 100 μL of complete DMEM. After 24 h, the cells were treated with the indicated compounds in the presence or absence of H_2O_2. After the treatments described, cells were incubated at 37 °C with 5% CO_2 for 24 h. To quantify cell viability, cell counting kit-8 (CCK-8,) assay was used. The culture medium was removed and the cells were washed twice with PBS. Subsequently, 100 μL of CCK-8 working solution was added to each well. The plate was then incubated at 37 °C for 1 h. Finally, absorbance was measured at 450 nm using a plate reader.

Tumor models

All experiment protocols involving animals were approved by the Institute of Materia Medica, Chinese Academy of Medical Sciences & Peking Union Medical College, the Animal Care & Welfare Committee, and the approval numbers are 00001743, IMM-S-25-0514 and IMM-S-25-0810. Healthy male C57BL/6 mice (6 weeks old, ~20 g) were purchased from Beijing Huafukang Bioscience Co., Ltd (Beijing, China), and raised in a specific-pathogen-free (SPF) barrier facility. Sex was not considered as a variable in this study. All the mice were housed in individually ventilated cages (IVCs) under a controlled barrier environment. The animal room was maintained at a constant ambient temperature of 23 ± 1 °C and relative humidity of 50 ± 20%, with a standard 12 h light/12 h dark cycle. Mice were provided with sterilized standard chow and autoclaved drinking water ad libitum. All animal experiments were performed in compliance with the Institutional Animal Care and Use Committee (IACUC) guidelines. Each mouse was subcutaneously injected with a suspension containing 1.5×10^6 MC38 cells in 100 μL solution into the right flank to establish a tumor-bearing mouse model. All tumors in the mice did not exceed the maximum size permitted by the ethics committee. The maximal permitted tumor size was 1500 mm^3, and the maximal tumor burden was restricted to ≤10% of the mouse's body weight, in line with the committee's ethical requirements for animal welfare. Tumor size was measured every 2 days using a digital caliper, and the volume was calculated with the formula: $V = 0.5 \times L \times W^2$ (where L = longest diameter, W = shortest diameter). If the tumor size or burden exceeded the above limits, or if the mice exhibited signs of distress, humane euthanasia was performed immediately.

Tumor inhibition test

When tumor volume reached about 50–100 mm^3, tumor-bearing mice were randomly divided into 7 groups ($n = 5$ biologically independent samples). The experimental group (G5) received an intraperitoneal injection of 28.74 μmol·kg^{-1} TCO-Dox **8**, followed by a subcutaneous injection of 115.21 μmol·kg^{-1} BTz **1** near the tumor after an interval of 20 min. For the other treatments, the interval between the two injections was maintained at 20 min. The mice received treatments on day 0 and day 3. Tumor volume and body weight were measured every 2 days. After 12 days, all mice were sacrificed.

Reporting summary

Further information on research design is available in the Nature Portfolio Reporting Summary linked to this article.

Data availability

Source Data are provided with this paper. The data that support the findings of this study are available within the paper and its Supplementary Information. All data supporting the findings of the study are available from the corresponding authors upon request.

References

1. Ji, X. et al. Click and release: bioorthogonal approaches to "on-demand" activation of prodrugs. *Chem. Soc. Rev.* **48**, 1077–1094 (2019).
2. Kozma, E., Bojtár, M., Hu, X. & Kele, P. Bioorthogonally assisted phototherapy: recent advances and prospects. *Angew. Chem. Int. Ed.* **62**, e202303198 (2023).
3. Flynn, R. A. et al. Small RNAs are modified with N-glycans and displayed on the surface of living cells. *Cell* **184**, 3109–3124.e3122 (2021).

4. Richter, D., Lakis, E. & Piel, J. Site-specific bioorthogonal protein labelling by tetrazine ligation using endogenous beta-amino acid dienophiles. *Nat. Chem.* **15**, 1422–1430 (2023).
5. Bumpus, T. W., Huang, S., Tei, R. & Baskin, J. M. Click chemistry-enabled CRISPR screening reveals GSK3 as a regulator of PLD signaling. *Proc. Natl. Acad. Sci. USA* **118**, e2025265118 (2021).
6. Hillman, A. S. et al. Minimalist tetrazine N-acetyl muramic acid probes for rapid and efficient labeling of commensal and pathogenic peptidoglycans in living bacterial culture and during macrophage invasion. *J. Am. Chem. Soc.* **146**, 6817–6829 (2024).
7. Xu, H. et al. On-membrane supramolecular assemblies serving as bioorthogonal gating for melphalan. *Angew. Chem. Int. Ed.* **64**, e202502922 (2025).
8. Yao, Q. et al. Reactive oxygen species-instructed supramolecular assemblies enable bioorthogonally activatable protein degradation for pancreatic cancer. *J. Am. Chem. Soc.* **147**, 18208–18218 (2025).
9. Kumar, G. S., Racioppi, S., Zurek, E. & Lin, Q. Superfast tetrazole-BCN cycloaddition reaction for bioorthogonal protein labeling on live cells. *J. Am. Chem. Soc.* **144**, 57–62 (2021).
10. Zhang, L. et al. Discovery of fluorogenic diarylsydnone-alkene photoligation: conversion of ortho-dual-twisted diarylsydnones into planar pyrazolines. *J. Am. Chem. Soc.* **140**, 7390–7394 (2018).
11. Nainar, S. et al. Temporal labeling of nascent RNA using photoclick chemistry in live cells. *J. Am. Chem. Soc.* **139**, 8090–8093 (2017).
12. McNitt, C. D., Cheng, H., Ullrich, S., Popik, V. V. & Bjerknes, M. Multiphoton activation of photo-strain-promoted azide alkyne cycloaddition "click" reagents enables in situ labeling with submicrometer resolution. *J. Am. Chem. Soc.* **139**, 14029–14032 (2017).
13. Mayer, S. V., Murnauer, A., von Wrisberg, M. K., Jokisch, M. L. & Lang, K. Photo-induced and rapid labeling of tetrazine-bearing proteins via cyclopropenone-caged bicyclononynes. *Angew. Chem. Int. Ed.* **58**, 15876–15882 (2019).
14. Arumugam, S. & Popik, V. V. Photochemical generation and the reactivity of *o*-naphthoquinone methides in aqueous solutions. *J. Am. Chem. Soc.* **131**, 11892–11899 (2009).
15. Feist, F. et al. Light-induced ligation of *o*-quinodimethanes with gated fluorescence self-reporting. *J. Am. Chem. Soc.* **142**, 7744–7748 (2020).
16. Adzima, B. J. et al. Spatial and temporal control of the alkyne-azide cycloaddition by photoinitiated Cu(II) reduction. *Nat. Chem.* **3**, 256–259 (2011).
17. Zhang, H. et al. Rapid bioorthogonal chemistry turn-on through enzymatic or long wavelength photocatalytic activation of tetrazine ligation. *J. Am. Chem. Soc.* **138**, 5978–5983 (2016).
18. Jemas, A. et al. Catalytic activation of bioorthogonal chemistry with light (CABL) enables rapid, spatiotemporally controlled labeling and no-wash, subcellular 3D-patterning in live cells using long wavelength light. *J. Am. Chem. Soc.* **144**, 1647–1662 (2022).
19. Wang, C. et al. Enabling in vivo photocatalytic activation of rapid bioorthogonal chemistry by repurposing silicon-rhodamine fluorophores as cytocompatible far-red photocatalysts. *J. Am. Chem. Soc.* **143**, 10793–10803 (2021).
20. Killops, K. L., Campos, L. M. & Hawker, C. J. Robust, efficient, and orthogonal synthesis of dendrimers via thiol-ene "click" chemistry. *J. Am. Chem. Soc.* **130**, 5062–5064 (2008).
21. Hensarling, R. M., Doughty, V. A., Chan, J. W. & Patton, D. L. "Clicking" polymer brushes with thiol-yne chemistry: indoors and out. *J. Am. Chem. Soc.* **131**, 14673–14675 (2009).
22. Singh, K. et al. Light harvesting for rapid and selective reactions: click chemistry with strain-loadable alkenes. *Chem* **4**, 124–137 (2018).
23. Li, J. et al. Visible light-initiated bioorthogonal photoclick cycloaddition. *J. Am. Chem. Soc.* **140**, 14542–14546 (2018).
24. Shah, L., Laughlin, S. T. & Carrico, I. S. Light-activated staudinger-bertozzi ligation within living animals. *J. Am. Chem. Soc.* **138**, 5186–5189 (2016).
25. Liu, L., Zhang, D., Johnson, M. & Devaraj, N. K. Light-activated tetrazines enable precision live-cell bioorthogonal chemistry. *Nat. Chem.* **14**, 1078–1085 (2022).
26. Chang, M. et al. Senolysis enabled by senescent cell-sensitive bioorthogonal tetrazine ligation. *Angew. Chem. Int. Ed.* **63**, e202315425 (2024).
27. Knittel, C., Chadwick, S., Kuehling, C. & Devaraj, N. K. Enzymatic activation of caged tetrazines for cell-specific bioconjugation. ChemRxiv https://doi.org/10.26434/chemrxiv-2024-78kxz (2024).
28. Wang, X. et al. Dual-locked enzyme-activatable bioorthogonal fluorescence turn-on imaging of senescent cancer cells. *J. Am. Chem. Soc.* **146**, 22689–22698 (2024).
29. Jiang, T. et al. Modular enzyme- and light-based activation of cyclopropene-tetrazine ligation. *ChemBioChem* **20**, 2222–2226 (2019).
30. Kumar, P., Jiang, T., Li, S., Zainul, O. & Laughlin, S. T. Caged cyclopropenes for controlling bioorthogonal reactivity. *Org. Biomol. Chem.* **16**, 4081–4085 (2018).
31. Kumar, P. et al. Caged cyclopropenes with improved tetrazine ligation kinetics. *Org. Lett.* **21**, 3721–3725 (2019).
32. Brevé, T. G. et al. Conditional copper-catalyzed azide-alkyne cycloaddition by catalyst encapsulation. *Angew. Chem. Int. Ed.* **59**, 9340–9344 (2020).
33. Cao, W. et al. Reversible control of tetrazine bioorthogonal reactivity by naphthotube-mediated host-guest recognition. *Chem* **9**, 2881–2901 (2023).
34. Lennicke, C. & Cochemé, H. M. Redox metabolism: ROS as specific molecular regulators of cell signaling and function. *Mol. Cell.* **81**, 3691–3707 (2021).
35. Snieckute, G. et al. ROS-induced ribosome impairment underlies ZAKα-mediated metabolic decline in obesity and aging. *Science* **382**, 6675 (2023).
36. Cheung, E. C. & Vousden, K. H. The role of ROS in tumour development and progression. *Nat. Rev. Cancer* **22**, 280–297 (2022).
37. Liu, J. et al. Reactive oxygen species (ROS) scavenging biomaterials for anti-inflammatory diseases: from mechanism to therapy. *J. Hematol. Oncol.* **16**, 116 (2023).
38. Deng, L. et al. The role of oxidative stress and antioxidants in diabetic wound healing. *Oxid. Med. Cell. Longev.* **2021**, 8852759 (2021).
39. Camargo, L. L., Rios, F. J., Montezano, A. C. & Touyz, R. M. Reactive oxygen species in hypertension. *Nat. Rev. Cardiol.* **22**, 20–37 (2024).
40. Butterfield, D. A. & Halliwell, B. Oxidative stress, dysfunctional glucose metabolism and Alzheimer disease. *Nat. Rev. Neurosci.* **20**, 148–160 (2019).
41. Bai, R., Guo, J., Ye, X.-Y., Xie, Y. & Xie, T. Oxidative stress: The core pathogenesis and mechanism of Alzheimer's disease. *Ageing Res. Rev.* **77**, 101619 (2022).
42. Wang, P., Gong, Q., Hu, J., Li, X. & Zhang, X. Reactive oxygen species (ROS)-responsive prodrugs, probes, and theranostic prodrugs: applications in the ROS-related diseases. *J. Med. Chem.* **64**, 298–325 (2021).
43. Yang, B., Chen, Y. & Shi, J. Reactive oxygen species (ROS)-based nanomedicine. *Chem. Rev.* **119**, 4881–4985 (2019).
44. Wu, H. & Devaraj, N. K. Advances in tetrazine bioorthogonal chemistry driven by the synthesis of novel tetrazines and dienophiles. *Acc. Chem. Res.* **51**, 1249–1259 (2018).
45. Oliveira, B. L., Guo, Z. & Bernardes, G. J. L. Inverse electron demand Diels–Alder reactions in chemical biology. *Chem. Soc. Rev.* **46**, 4895–4950 (2017).

46. Lin, F. et al. Multimodal targeting chimeras enable integrated immunotherapy leveraging tumor-immune microenvironment. *Cell* **187**, 7470–7491 (2024).
47. Czuban, M. et al. Bio-orthogonal chemistry and reloadable biomaterial enable local activation of antibiotic prodrugs and enhance treatments against Staphylococcus aureus infections. *ACS Cent. Sci.* **4**, 1624–1632 (2018).
48. Chawla, S. P. et al. Interim phase 1 results for SQ3370 in advanced solid tumors. *J. Clin. Oncol.* **40**, 3085–3085 (2022).
49. Blackman, M. L., Royzen, M. & Fox, J. M. Tetrazine ligation: fast bioconjugation based on inverse-electron-demand Diels-Alder reactivity. *J. Am. Chem. Soc.* **130**, 13518–13519 (2008).
50. Devaraj, N. K., Weissleder, R. & Hilderbrand, S. A. Tetrazine-based cycloadditions: application to pretargeted live cell imaging. *Bioconjug. Chem.* **19**, 2297–2299 (2008).
51. Versteegen, R. M., Rossin, R., ten Hoeve, W., Janssen, H. M. & Robillard, M. S. Click to release: instantaneous doxorubicin elimination upon tetrazine ligation. *Angew. Chem. Int. Ed.* **52**, 14112–14116 (2013).
52. Hoshi, K., Messina, M. S., Ohata, J., Chung, C. Y.-S. & Chang, C. J. A puromycin-dependent activity-based sensing probe for histochemical staining of hydrogen peroxide in cells and animal tissues. *Nat. Protoc.* **17**, 1691–1710 (2022).
53. Chang, M. C., Pralle, A., Isacoff, E. Y. & Chang, C. J. A selective, cell-permeable optical probe for hydrogen peroxide in living cells. *J. Am. Chem. Soc.* **126**, 15392–15393 (2004).
54. Wang, J. et al. Tumor-targeted oxaliplatin(IV) prodrug delivery based on ROS-regulated cancer-selective glycan labeling. *J. Med. Chem.* **67**, 8296–8308 (2024).
55. Innes-Gold, S., Cheng, H., Liu, L. & Cohen, A. E. Tools for intersectional optical and chemical tagging on cell surfaces. *ACS Chem. Biol.* **20**, 455–463 (2025).
56. Oka, N., Yamada, T., Sajiki, H., Akai, S. & Ikawa, T. Aryl boronic esters are stable on silica gel and reactive under Suzuki–Miyaura coupling conditions. *Org. Lett.* **24**, 3510–3514 (2022).
57. Lebraud, H., Wright, D. J., Johnson, C. N. & Heightman, T. D. Protein degradation by in-cell self-assembly of proteolysis targeting chimeras. *ACS Cent. Sci.* **2**, 927–934 (2016).
58. Chang, M. et al. Bioorthogonal PROTAC prodrugs enabled by on-target activation. *J. Am. Chem. Soc.* **145**, 14155–14163 (2023).
59. An, K. et al. Stimuli-responsive PROTACs for controlled protein degradation. *Angew. Chem. Int. Ed.* **62**, e202306824 (2023).

Acknowledgements

This work was supported by the Non-profit Central Research Institute Fund of Chinese Academy of Medical Sciences to L.L. (2022-RC350-02), CAMS Innovation Fund for Medical Sciences (2023-I2M-QJ-011, 2021-I2M-3-001, 2021-I2M-1-026 and 2023-I2M-2-006), National Natural Science Foundation of China (Nos. 82404404), Beijing Nova Program to L.L. (No. 2022048), and the Fundamental Research Funds for Central Universities. Peking Union Medical College to J.Z. (3332024067).

Author contributions

L.L. and D.M. conceived the project. D.M., B.M., and D.P. designed and performed the synthetic experiments. D.M., J.Z., W.W., and L.C. conducted the targeted protein degradation experiments. D.M., J.Z., Y.K., and Y.W. conducted the cell and mouse experiments. D.M., B.M., J.Z., and L.L. analyzed the data. L.L., J.Z., and D.M. wrote the manuscript. L.L. and R.W. supervised the project.

Competing interests

The authors declare no competing interests.

Additional information

Supplementary information The online version contains supplementary material available at https://doi.org/10.1038/s41467-026-68771-z.

Correspondence and requests for materials should be addressed to Rui Wang or Luping Liu.

Peer review information *Nature Communications* thanks Yuan Gao, Tao Liu and the other anonymous reviewer for their contribution to the peer review of this work. [A peer review file is available].

Reprints and permissions information is available at http://www.nature.com/reprints

Publisher's note Springer Nature remains neutral with regard to jurisdictional claims in published maps and institutional affiliations.

Dongqing Ming[1,3], Jiaxue Zhang[1,3], Binsong Mu[1,3], Dongxue Peng[1], Yanjun Wang[1], Yangyang Kong[1], Wenjing Wang[2], Ling Chu[2], Rui Wang[1] ✉ & Luping Liu[1] ✉

[1]State Key Laboratory of Bioactive Substance and Function of Natural Medicines, Institute of Materia Medica, Chinese Academy of Medical Sciences & Peking Union Medical College, Beijing, PR China. [2]School of Pharmaceutical Sciences, Tsinghua University, Beijing, PR China. [3]These authors contributed equally: Dongqing Ming, Jiaxue Zhang, Binsong Mu. ✉e-mail: wangrui@imm.ac.cn; lpliu@imm.ac.cn